Particle Accelerators, 1994, Vol. 48, pp. 109–134
Reprints available directly from the publisher
Photocopying permitted by license only

CONTINUOUS TRANSMISSION LINE MODELING OF A DTL INCLUDING BEAM LOADING AND OTHER PERTURBATIONS

M.K. KE, B.R. CHEO and J. SHMOYS

Weber Research Institute, Polytechnic University, Farmingdale, New York 11735, USA

(Received 6 December 1993; in final form 15 June 1994)

The rf structure of a DTL is first modeled by a circular waveguide filled with an anisotropic medium with scalar permeability μ and tensor permittivity $\bar{\bar{\varepsilon}} = \hat{\mathbf{z}}\hat{\mathbf{z}}\varepsilon_z + \hat{\mathbf{r}}\hat{\mathbf{r}}\varepsilon_t$. The two structures are equivalent in four pertinent characteristics from which the waveguide parameters and a radius a are determined. The exact geometry of the DTL including the facing angles, the beam holes and the stems is used in the process via SUPERFISH computations. A transmission line modeling the waveguide is then established, which is further improved to include the first order effects of structure losses, beam loading and external rf sources. Comparisons with experimental results are favorable.

KEY WORDS: Linear accelerators, radio-frequency devices

1 INTRODUCTION

The development of computer codes in recent years has enabled the accelerator designers to obtain accurately a cell by cell design of a drift tube linac (DTL) including the effect of the details of cell geometry and the parameters of the beam. The purpose of the present paper is to provide an analytic background which integrates the information obtained in the cell-by-cell design to form a realistic and comprehensive 1-D model, capable of predicting the global and dynamic behavior of a DTL tank and its interactions with external rf sources. The emphasis will be on the rf field profile in both amplitude and phase along the length of the accelerator tank, as reacting to various forms of perturbations. It can also serve as an additional tool, parallel to the cold model experiments, providing information of interest for the final hot model design.

For practical range of energy levels of DTL's, the cell length is usually small compared with wavelength. At 85 MeV protons, $\beta \cong 0.4$ and $\beta \cong 0.2$ for 25 MeV protons. Thus one may surmise that the DTL tank may be considered as a circular waveguide periodically loaded by drift tubes. The global behavior of the tank is then that of the loaded waveguide terminated at the ends. The rippled field near the drift tubes can be considered as the perturbations and its effects would be revealed through the dispersion relation of

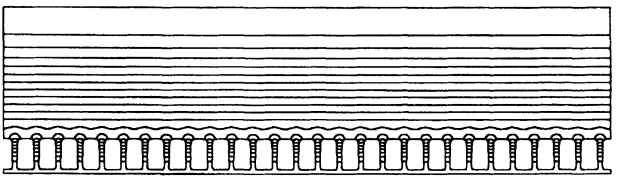

(a) A constant-β drift tube linac

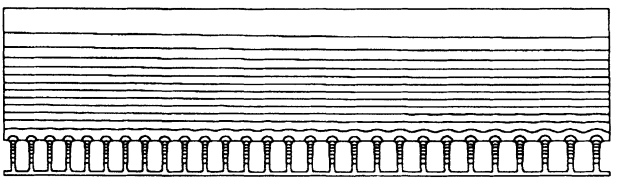

(b) A graded-β drift tube linac

FIGURE 1: The equipotential lines of the magnetic field for TM_{010}-like mode in a constant DTL and a graded-β DTL.

the loaded guide. The field line distribution of a DTL obtained from SUPERFISH[1] code supports this view (Figure 1). Further, one may see that the higher order Floquet modes decay very rapidly away from the axis, approximately as $\exp(-n\pi r/\beta\lambda)$. The main Floquet mode, which takes the form as that of the TM_{01} mode of circular waveguide, should thus characterize the dispersion relation and the macroscopic behavior of the tank. This approach of analyzing periodic rf structures has been used successfully for many years in the microwave tube community.

An earlier attempt[2] was made to represent a linac as a cascade of coaxial and circular waveguide transmission lines. Interesting features, such as ramp generation and stabilization by post couplers of a DTL tank could be observed, and were in general agreement with experimental results. However, the drawback of this approach is that in the operating energy level of most DTL's, the lengths of the sections are very small compared with wavelength. The number of modes required for each section is excessive, rendering the approach impractical.

In this paper, we follow the approach used in the transmission line modeling of an RFQ,[3] and propose that the basic rf structure of a drift tube linac can be modeled by a circular waveguide filled by a medium with a uniaxial, rather than isotropic,[4] dielectric $\bar{\bar{\varepsilon}} = \hat{\mathbf{z}}\hat{\mathbf{z}}\varepsilon_z + \hat{\mathbf{r}}\hat{\mathbf{r}}\varepsilon_t$ where $\hat{\mathbf{z}}$ and $\hat{\mathbf{r}}$ are unit vectors, and with scalar permeability μ. The two structures are equivalent in all principal characteristics relevant to the operations of an accelerator. Exact relations between the two structures are presented later in Section 3. The four parameters of the waveguide μ, ε_z, ε_t, and radius a, are determined numerically via SUPERFISH Code calculations for a practically designed DTL geometry including effects of drift tube stems, facing angles, beam holes, etc. This waveguide is then further represented by a transmission line via standard techniques leading to a pair of transmission

line equations. Energetic relations, the energy stored, ohmic wall losses (shunt impedance) and beam loading effects are then incorporated into the transmission line model. Based on this model, the effects of post couplers including those for a ramped gradient DTL can also be analyzed.[5]

Sections 2–4 represent the procedure in obtaining the transmission line parameters of the basic rf structure. This is followed in Sections 5–6, by the energetic relations corresponding to the actual operating conditions of the accelerator tank. Thus the model predicts accurately the tank's performance in its dispersion relation, rf power flow, energy gain, power gain and energy stored, and the effects on the rf drive sources. Thus it also gives accurately the resonant frequency shift and the Q factor of the tank due to the beam loading. These factors are becoming more important as superconducting structures have become a reality. Section 7 presents the test of the basic model as compared with multicell SUPERFISH calculations and cold model experiments with extremely satisfying accuracy. Section 8 provided an analysis of the post couplers in the context of the model.

2 PROPAGATION CHARACTERISTICS IN WAVEGUIDE FILLED WITH ANISOTROPIC DIELECTRIC

The electromagnetic field in an azimuthally symmetric transverse magnetic $(TM)_{0n}$ mode in a circular waveguide filled with a medium with scalar permeability μ and uniaxial permittivity $\bar{\bar{\varepsilon}} = \hat{\mathbf{z}}\hat{\mathbf{z}}\varepsilon_z + \hat{\mathbf{r}}\hat{\mathbf{r}}\varepsilon_t$ are expressed in terms of electric and magnetic mode functions, $\mathbf{e}(r)$ and $\mathbf{h}(r)$, which describe the transverse behavior of transverse fields[6]. These mode functions are related

$$\mathbf{h} = \hat{\mathbf{z}} \times \mathbf{e} \tag{1}$$

where $\hat{\mathbf{z}}$ is a unit vector in the axial direction, and normalized over the cross-section

$$\int\int_{\substack{\text{Cross}\\ \text{Sections}}} |\mathbf{e}|^2 dS = 1 \tag{2}$$

The mode function satisfies the transverse wave equation

$$\nabla_t^2 \mathbf{e}(r) + k_c^2 \mathbf{e}(r) = 0 \tag{3}$$

and appropriate boundary condition at the wall, $\hat{\mathbf{r}} \times \mathbf{e} = 0$. The mode function $\mathbf{e}$ is given by

$$\mathbf{e}(r) = \hat{\mathbf{r}} \frac{J_1(\chi r/a)}{\sqrt{\pi} J_1(\chi)} \tag{4}$$

where $\hat{\mathbf{r}}$ is a unit vector in the radial direction, a is the radius of the waveguide, and $\chi \cong 2.405$ is the lowest root of $J_0(\chi) = 0$. The cut-off wavenumber k_c for this mode is χ/a. The transverse fields are then

$$\mathbf{E}_t = V(z)\mathbf{e}(r) \tag{5a}$$

$$\mathbf{H}_t = I(z)\mathbf{h}(r) \tag{5b}$$

The voltage and current functions, $V(z)$ and $I(z)$, satisfy, as result of Maxwell's equations, transmission line equations

$$-\frac{dV(z)}{dz} = (j\omega\mu + k_c^2/j\omega\varepsilon_z)I(z) \tag{6a}$$

$$-\frac{dI(z)}{dz} = j\omega\varepsilon_t V(z) \tag{6b}$$

The 'per unit length' circuit representation of this transmission line is shown in Figure 2, the series distributed impedance being $(j\omega\mu + k_c^2/j\omega\varepsilon_z)$ and shunt admittance $j\omega\varepsilon_t$. The propagation constant is then

$$\gamma = \sqrt{-\omega^2\varepsilon_t\mu + k_c^2\varepsilon_t/\varepsilon_z} \tag{7a}$$

and the characteristic impedance

$$Z_0 = \sqrt{\frac{\mu}{\varepsilon_t} - \frac{k_c^2}{\omega^2\varepsilon_t\varepsilon_z}} \tag{7b}$$

At cutoff, i.e. when $\omega = k_c/\sqrt{\mu\varepsilon_z}$, $\gamma = 0$, and, depending on boundary conditions at the two ends, the field distribution is either a constant or a linear ramp. From Equations (6a) and (6b), $dV/dz = 0$ leads to $V = C_1$, $I = -j\omega\varepsilon_z C_1 z + C_2$. Axial magnetic field is zero, since this is a TM mode, and axial electric field is

$$E_z = I\frac{\nabla_t \cdot \mathbf{e}}{j\omega\varepsilon_z} = I\frac{\chi J_0(\chi r/a)}{j\omega\varepsilon_z\sqrt{\pi}a^2 J_1(\chi)} \tag{8}$$

Note that the axial electric field is proportional to transmission line current.

3 EQUIVALENT WAVEGUIDE

To model a DTL by an equivalent waveguide filled with a uniaxial dielectric, we must find the four parameters characterizing such a waveguide, its radius a, the transverse and axial permittivities ε_t and ε_z, and permeability μ. This can be done by imposing that four characteristics of fields in a unit cell match the corresponding characteristics of the waveguide. The goal is that with the parameters set in this manner, the cell by cell behavior of the transmission line equivalent will accurately approximate that of the DTL over a range of frequencies in the neighborhood of the operating frequency.

The four characteristics used in this paper,

1. cutoff frequency
2. axial impedance in the TM_{010} mode
3. propagation constant in the next higher order axial mode TM_{011}
4. transverse impedance in the same mode as in 3,

did yield a successful model, as is shown below. Let us then go through the four conditions listed above and see how we can extract the values a, ε_t, ε_z, and μ from them.

A typical unit cell is shown in Figure 3. Condition (1) sets the cut-off frequency of the waveguide equal to the resonant frequency of the unit cell, ω_c, i.e.

$$\frac{2.405}{a\sqrt{\mu\varepsilon_z}} = \omega_c \tag{9}$$

Condition (2) stipulates that at $\omega = \omega_c$ the ratio $E_z(z, 0)/H_\phi(z, a)$ be equal to the ratio of the corresponding quantities in the unit cell, when they are averaged over the length of the unit cell. Since this field ratio in the equivalent waveguide at $\omega = \omega_c$, is $-j\sqrt{\mu\varepsilon_z}J_0(0)/J_1(2.405)$, we have

$$\sqrt{\frac{\mu}{\varepsilon_z}}\,\frac{J_0(0)}{J_1(2.405)} = \frac{\int_0^L E_z(z, 0)dz\Big|_{DTLcell}}{\int_0^L H_\phi(z, a)dz\Big|_{DTLcell}} \tag{10}$$

where the field values in the right hand side are obtained from SUPERFISH computation for the unit cell.

For the remaining conditions we pick the next higher axial mode in a multicell structure and run SUPERFISH for this mode. The propagation constant γ_{011} of this mode is then purely imaginary, $\gamma_{011} = j\beta_{011}$ and the phase length of the cavity, π, can be equated to the phase length of the equivalent transmission line, so that

$$\gamma_{011} = j\beta_{011} = \sqrt{(\omega_c^2 - \omega_1^2)\,\mu\varepsilon_t} = j\pi/d \tag{11}$$

where β_{011} is the phase constant, ω_1 the resonant frequency of the next higher order axial mode, obtained from SUPERFISH, and d is the total length of the multicell structure.

For the last condition we extract from the SUPERFISH computation the maximum values of the transverse electric field E_r and magnetic field H_ϕ at the tank wall; the ratio of the two gives the transverse impedance, which is set equal to the corresponding quantity in the equivalent waveguide

$$Z_{01} = \sqrt{\frac{\mu}{\varepsilon_t}}\sqrt{1 - \frac{\omega_c^2}{\omega_1^2}} = \frac{|E_r(z, a)|_{\max}}{|H_\phi(z, a)|_{\max}} \tag{12}$$

Equations (9)–(12) yield the values of the four parameters needed. As we can see, μ and ε_t can be obtained from equations (11) and (12), then e_z from Equation (10) and finally, the equivalent waveguide radius a from Equation (9).

As it is apparent, for whatever reason, intentional or not, these parameters can all be functions of z, and the model as given by the equations (6a) and (6b) can deal with this situation. It can predict the overall structure resonant frequency, the perturbation to the field profile, and some other issues concerning the RF structure behavior.

4 EFFECT OF STEMS

Since stems are as closely spaced as drift tubes, their effect should be incorporated into the waveguide model. As stems are located in a region of low transverse electric field, their effect is small and manifests itself primarily in expelling the magnetic field from the volume occupied by the stems. Hence, we will consider their effect to be a perturbation of the magnetic permeability of the medium filling the equivalent waveguide. The perturbation of the resonant frequency of a DTL by a stem is calculated in SUPERFISH using Slater's perturbation theorem

$$\frac{\Delta\omega_c}{\omega_c} \approx \frac{\int_{\Delta V} \left(\mu|H|^2 + \varepsilon|E|^2\right) d\tau}{\int_{V} \left(\mu|H|^2 + \varepsilon|E|^2\right) d\tau} \tag{13}$$

Translating this change in the cut-off frequency into a revised magnetic permeability μ'

$$\mu' = \frac{k_c^2}{\omega_c'^2 \varepsilon_z} \tag{14}$$

where k_c remains unchanged since it depends on waveguide dimensions only and $\omega_c' = \omega_c + \Delta\omega_c$. Transmission line equations remain as in (6), except that μ is replaced by μ'.

5 STRUCTURE LOSSES AND BEAM LOADING

In preceding sections, we established for the RF structure of a DTL, a transmission line model, corresponding to that of a circular waveguide filled with a uniaxial dielectric. In this section and the next we shall improve the model to include first order effects. As implied in the fact that the transmission line parameters may be functions of position, the model is thus capable of dealing with various issues in the cavity field distribution due to geometric perturbation of the tank. One of the issues, ramp generation, is shown in section 7 as a test of this model against experiments. The next first order effect is due to structure losses and beam loading and it is of the order of Q^{-1}. The goal of this section is to incorporate these effects into the transmission line model; thus the external rf drive sources must also be included. The effect of the beam dynamics on the cavity field is implicitly included in the data of the beam power, phase spread and synchronous phase, i.e. the determination of the fundamental Fourier component of the beam current as it is incorporated into the model.

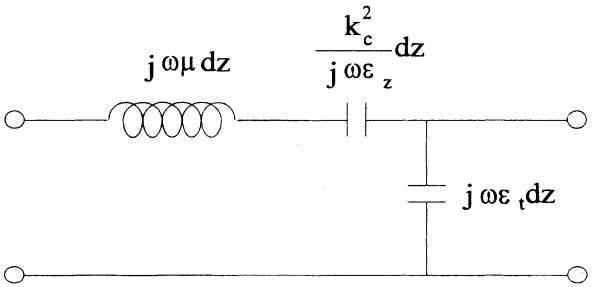

FIGURE 2: The equivalent circuit for TM mode.

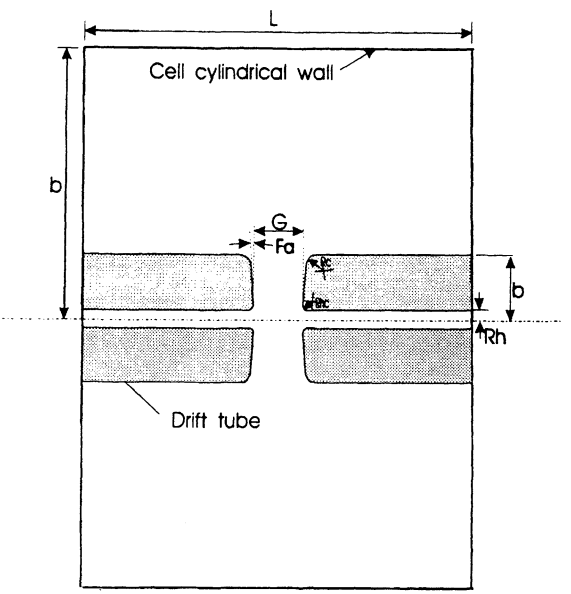

FIGURE 3: A unit cell of the DTL.

A) Structure ohmic losses: The effect of RF power dissipated in the cavity walls and drift tubes can be represented by a distributed resistance in the equivalent circuit Figure 2 in series with the series inductance $j\omega\mu dz$ or, alternately, as a shunt conductance G across the capacitive reactance $\left(k_c^2/j\omega\varepsilon_z\right) dz$. In the latter case, it corresponds to the shunt impedance of the cavity. These are shown in Figure 4a and 4b. In typical designs the numerical values of R and G are small compared with $\omega\mu$ and $\left(\omega\varepsilon_z/k_c^2\right)$ respectively. The dimension of R is ohms per meter while that for G is in mhos-meter, same as that of $\left(\omega\varepsilon_z/k_c^2\right)$. G^{-1} is thus a large quantity in ohms/meter, and is proportional to the

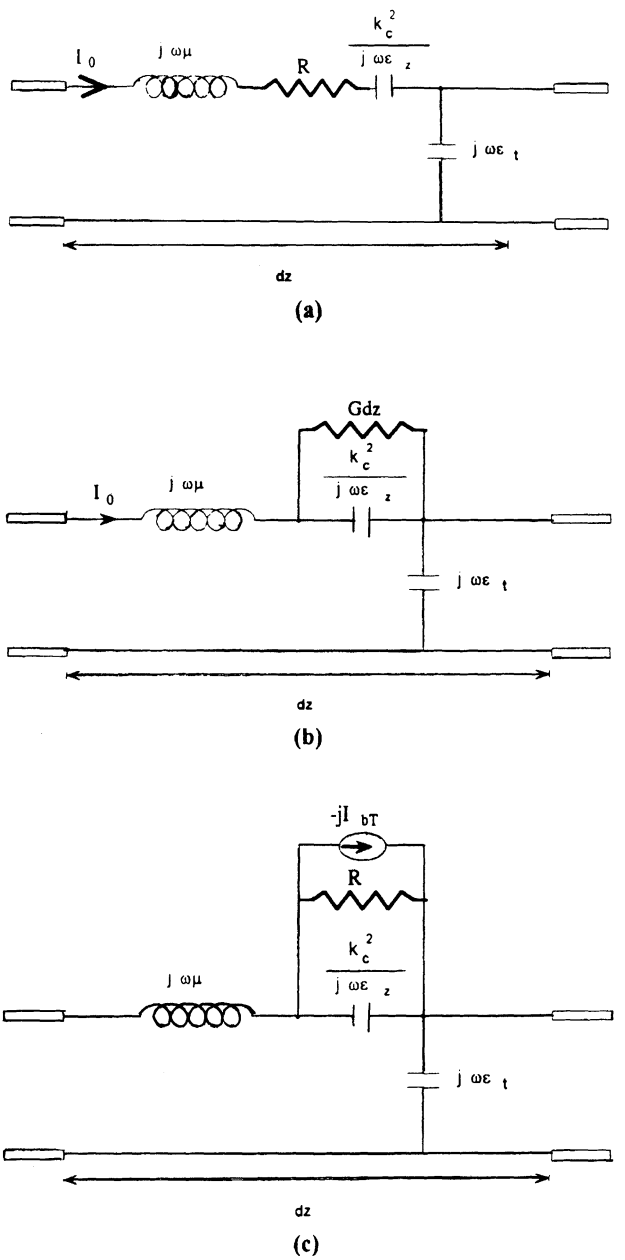

FIGURE 4: The equivalent circuits of the DTL including beam loading and wall losses.

shunt impedance of the structure. Recall that at resonance $\omega\mu = k_c^2/\omega\varepsilon_z$, the values of $\omega\mu/R$ and $(\omega\varepsilon_z/k_c^2 G)$ are equal to the Q factor of the cell, which is available in the design codes such as the SUPERFISH.

B) Beam loading effects: The charge particle beam in a DTL, or any other RF accelerator, is most accurately represented by a 3-D phase space description. The first order effect is that the beam bunches, or micro pulses, traveling along the accelerator represent a periodic current which may vary moderately along the length of the accelerator. The fundamental Fourier component of this current interacts with the RF field and effects the power transfer. It is to be noted that the beam bunches occur at the synchronous phase of the RF field. Therefore the ac-ac interaction consists of both an inphase component and a quadrature component. The former results in real power transfer while the latter produces reactive power resulting in cavity detuning. In the following we present a procedure for including the effect of the beam into the model. The phasor current I_b, representing the effects of beam loading, shall be represented as a current generator connected in parallel with $k_c^2/j\omega\varepsilon_z$ and G as shown in Figure 4c[7]. It is understood that when the beam is present in the structure, the cavity is at the operating condition, with each parameter near its design value. Information needed in this procedure is: at each cell, the energy stored, the beam current, the beam power, the synchronous phase and the averaged E field (E_0); all can be obtained from the standard design codes.

The energy stored per cell U is used to normalize the model at the operating condition: $U = \mu|I_0|^2 L/2$, where L is the cell length. $|I_0| = (2U/\mu L)^{1/2}$ thus determining voltages and currents, $V(z)$ and $I(z)$, at the design values. Since $G \ll j\omega\varepsilon_z/k_c^2$, and, as shall be seen later, $|I_b| \ll |I_0|$, the voltage $dV_0 = I_0(k_c^2/j\omega\varepsilon_z)dz$ is related to E_z as seen from Equation 7, and E_z is proportional to $I_0(k_c^2/j\omega\varepsilon_z)$. The phasor current I_b represents the effect of beam loading in that the power absorbed by the particle beam is set to equal to that absorbed by I_b. For convenience we use the phase of E_0 as reference, then $E_0 = |E_0|$ and $I_0 = j|I_0|$. Let the complex beam power per unit length be defined as

$$W_b(z) = \frac{1}{2}\iint_{\substack{\text{cross}\\ \text{section}}} \mathbf{J}\cdot\mathbf{E}^* dS = P_b(z) + jQ_b(z) \quad \text{W/m} \tag{15}$$

where $\mathbf{J}$ is the phasor of the fundamental Fourier component of the beam current density, P_b is the beam power in a cell divided by the cell length and is available from the design data and Q_b is the so-called reactive power. Integrating,

$$W_b = \frac{1}{2} I_b |I_0| k_c^2/\omega\varepsilon_z \tag{16}$$

Since[a]

$$I_b = |I_b| e^{j\phi s} = I_{bi} + jI_{bq} \ (\phi_s = \text{ synchronous phase}) \tag{17}$$

[a] In this paper we use the phasor notation corresponding to $e^{j\omega t}$ time variation. Thus $|I_0|e^{j\phi s}$ represents a current with peaks at ϕ_s before the peaks of the accelerating field.

where I_{bi} and I_{bq} are respectively the inphase and quadrature components of I_b. Hence $Q_b = P_b \tan \phi_s$, and

$$I_b = \frac{2P_b\omega\varepsilon_z}{I_0 k_c^2}(1 + j \tan \phi_s) \tag{18}$$

We note that the per unit length voltage $I_0\left(k_c^2/j\omega\varepsilon_z\right)$ is proportional to $< E_z >$ (the "E_0"), G^{-1} is therefore proportional to shunt impedance (both in ohms per meter). It should be emphasized that the above calculation is predicated on the assumption that the perturbation due to ohmic losses is small. The same assumption will be made about beam loading, i.e. the effective value of the Q factor is sufficiently high when beam loading is also taken into consideration.

6 CAVITY EXCITATION

Having discussed the representation of rf power consumed by structure and the beam in drift tube linacs, we now come to the circuit models of generators which provide this power,[8,9] Linacs are ordinarily excited through slots or loops.

In the case of a slot feed shown in Figure 5a, for the purpose of calculating the equivalent network, we may close the aperture with a perfect conductor; the electric field $\mathbf{E}$ which exists in the aperture is recreated by equivalent magnetic surface currents $\mathbf{M} = \pm\hat{\mathbf{r}} \times \mathbf{E}$, equal and opposite, on both sides of the closed off aperture.[6] Since the electric field in the aperture must be axial, the equivalent magnetic current is azimuthal. Since the axial extent of the aperture is small compared[3] to wavelength, the magnetic current can be thought of as concentrated in a single cross-section of the linac. A distribution of magnetic current over the cross-section of the tank waveguide implies a discontinuity of electric field with continuous magnetic field, and hence a series element in the transmission line representing the dominant mode, as shown in Figure 5c. In addition, the excitation of higher order modes by this magnetic current results in local energy storage represented in Figure 5c by a reactance. On the feed waveguide side, similar considerations apply, yielding the picture of transformer coupled transmission line terminating in a generator with internal impedance Z_g. Other networks, for impedance matching etc., may be inserted in the feed transmission line.

Similar considerations apply in the case of a loop feed shown in Figure 5d. The current of the coaxial line feed flows through the loop located in an axial plane. The current loop is equivalent to an azimuthal magnetic dipole. Assuming, as is normally the case, that the axial extent of the loop is small, we have again a discontinuity in the transverse electric field or voltage with continuous magnetic field over the cross-section of the linac, resulting in the same equivalent network as in Figure 5c.

Using the modeling approaches given here and in section 5, effects such as the detuning by the beam and the cavity field phase variations along the length of the structure can be calculated. The procedure is same as that demonstrated in the earlier RFQ modeling paper.[3]

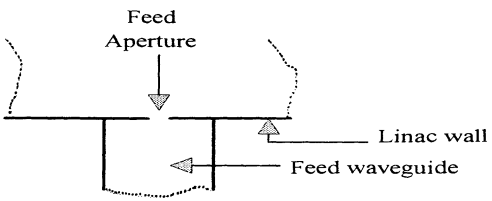

Figure 5(a)

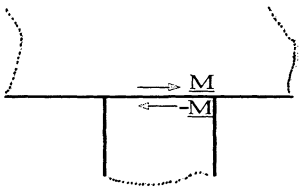

Figure 5(b)

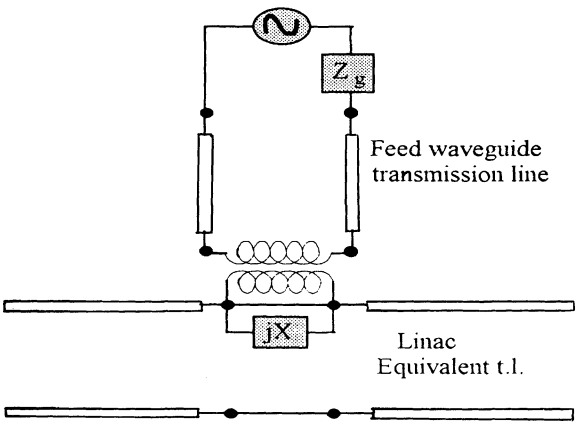

Figure 5(c)

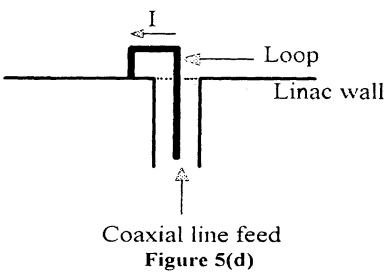

Figure 5(d)

FIGURE 5: Cavity feed structure and equivalent circuit.

TABLE 1: The geometry of a scale model for testing

	Constant-β Model
Frequency	427 MHz
Number of cells	47
Tank diameter	42.276 cm
Drift-tube diameter	8.954 cm
Bore diameter	0.824 cm
Average cell length	4.556 cm
Average drift-tube length	3.654 cm
Average gap length	0.911 cm
Overall tank length	214.15 cm
Face angle	3.0°
Stem diameter	1.588 cm
Post-coupler diameter	1.111 cm

7 TESTING THE TRANSMISSION LINE MODEL

A number of tests of the model were run on the constant β structure used in the experimental study of Billen and McMurry[10] the parameters of the structure are shown in Table 1. Some of these tests are comparisons of results obtained from the waveguide model with SUPERFISH calculations for the structure; others are comparisons with experimental results. Some comparison is also made with the Grumman Continuous Wave Deuteron Demonstrator (CWDD), Ramp Gradient DTL (RGDTL) cold test.[11]

The dispersion curve of the waveguide model is compared with SUPERFISH results in Figure 6. The effect of stems in this case has been omitted. One way to compare the model with the actual structure is by comparing tilt sensitivity. This is obtained in the actual structure by displacing one end of the cavity, changing the resonant frequency by a perturbation of Δf (see Figure 7a and b) than displacing the opposite end of the cavity until the original resonant frequency f_0 is restored. The effect of this is to create a linear ramp. For small perturbations the ramp is proportional to the frequency perturbation. Ramp sensitivity, S, is defined in terms of the voltages of first cell V_1 and last cell, V_N,

$$S = \frac{V_N - V_1}{V_N + V_1} \times 200\% \tag{19}$$

where the cell voltage is defined as the integral of E_z along the axis over the length of that cell. In the transmission line model, moving the cavity wall can be simulated by terminating

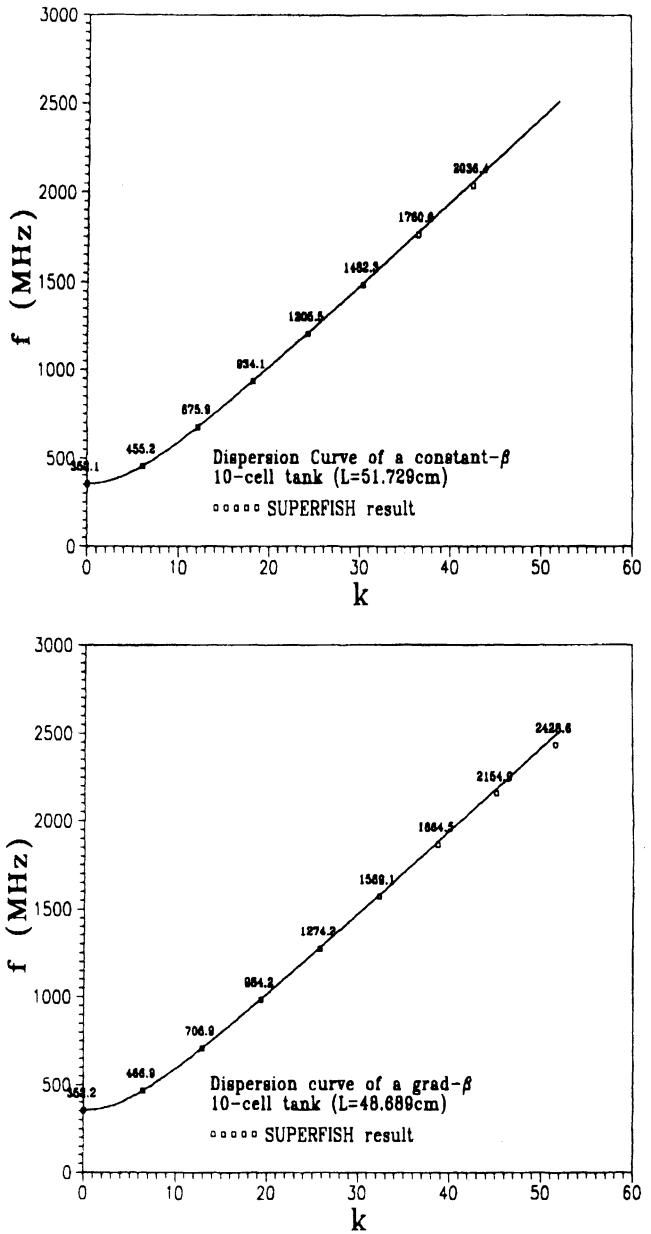

FIGURE 6: The dispersion curves of a constant-β DTL. Bottom: the dispersion curve of a gradient-β DTL.

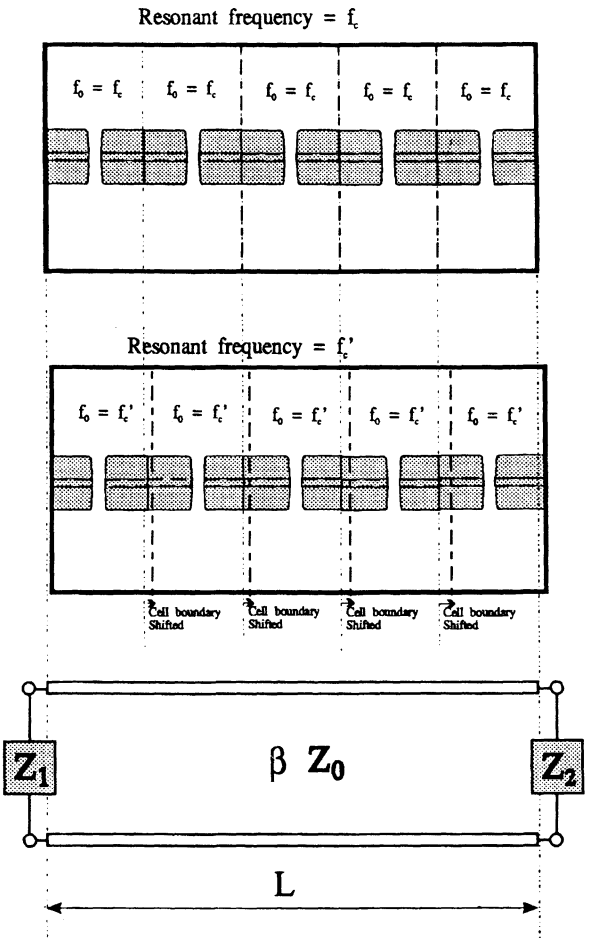

FIGURE 7: Modeling the procedures of the ramp creation by a transmission line.

the transmission line in a reactance (cf. Figure 7c) The procedure is very much the same. The resonant frequency is changed by Δf by replacing the short circuit by an appropriate reactance at one end, and then brought back to the original value by replacing the short circuit by a reactance at the opposite end. For a uniform structure, at resonance

$$j\omega\mu - k_c^2/j\omega\varepsilon_z = 0 \tag{20}$$

so that in the transmission line model, $V(z)$ the voltage is constant. With short circuit terminations, $E_r(z) = 0$ and hence $V(z) = 0$. With reactive terminations jX_1 and jX_2, $V(z) \neq 0$, but still constant. From the second transmission line equation (6b) it follows that $I(z)$ is a linear function for the transmission line model. Ramp sensitivity is defined in

TABLE 2: Calculation results compare to experimental data (without stems)

Perturbation Frequency	ε_t	ε_z	μ	X_1	X_2	Model Ramp (%)	Experiment Ramp (%)
200kHz	1.0001	0.9270	1.0119	–12.513	7.644	47.280	42.00
320kHz	0.9998	0.9270	1.0122	–23.275	10.654	72.816	67.20
475kHz	0.9994	0.9270	1.0125	–44.415	13.621	103.86	99.75
At cutoff	1.0006	0.9270	1.0114	0	0	0	0

very much the same way as for the linac itself, with first and last cell voltages replaced by transmission line currents at the two terminations.

The ramp, as obtained by using SUPERFISH on the structure of Table 1, but omitting stems, is shown in Figure 8. The somewhat uneven curve is due to marginal mesh size imposed on us by the limitations of our computer (in addition we had to limit the length of the linac to 20 cells). The corresponding curves for the transmission line model are shown in Figure 9. The current is normalized to unity at the midpoint in all cases. The resulting ramp for $\Delta f = 475$ kHz is 17.9% for the SUPERFISH results and 18.9% for the equivalent transmission line. The results for the full 47 cell linac, using the transmission line model, and comparison with the experimental results of Billen and McMurry[7] are shown in Table 2. We see that there is a discrepancy of 6–9%. This is due largely to the fact that the transmission line model neglected the effect of stems. The model was then improved by introducing their effect (perturbing μ) to all cells except the end cells, as in the linac used by Billen and McMurry. The comparison for this case is in Table 3, showing extremely close agreement. It is seen that in Table 2, the parameters ε_z, ε_t, and μ vary slightly for different perturbation frequencies. This variation is due to the slight change of the cell geometry resulting from the end wall shifting.[12]

The transmission line model was also constructed for the RGDTL CWDD constructed by Grumman Space System Division.[8] Since this is a variable β structure, the effect of stems differs from cell to cell, leading to a model using a non-uniform transmission line.

TABLE 3: Result comparison (with stems)

Perturbation Frequency	X_1	X_2	Tilt Sensitivity (%)	Ramp (%)	Experiment Ramp (%)
200kHz	–11.805	7.742	218.94	43.788	42.00
320kHz	–21.779	10.762	216.32	69.239	67.20
475kHz	–40.966	13.725	210.67	100.067	99.75
at f_0'	0	0	0	0	0

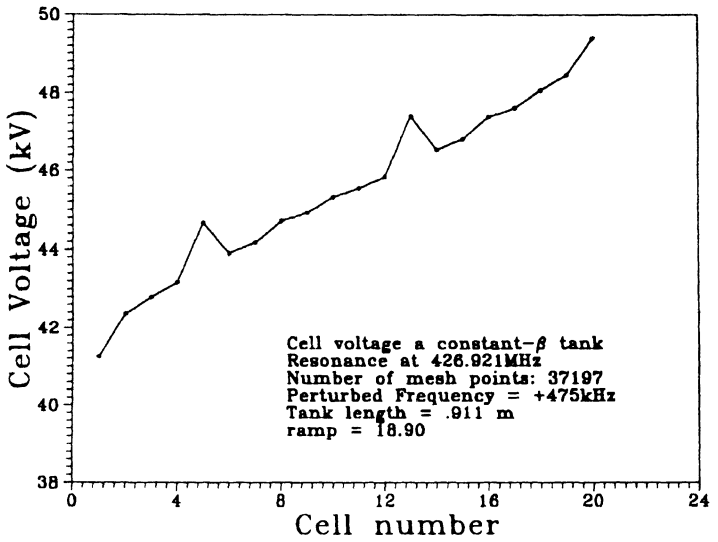

FIGURE 8: SUPERFISH result: cell voltages.

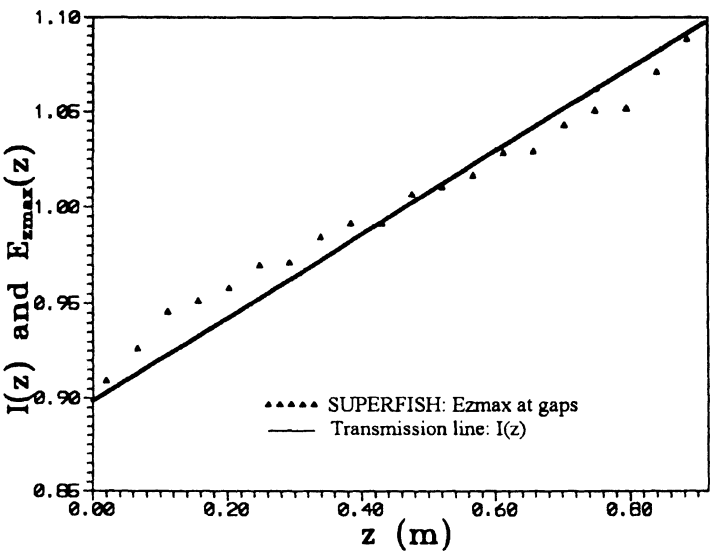

FIGURE 9: The result comparison of the transmission line model and SUPERFISH.

TABLE 4: The geometry of a CWDD

	CWDD Design
Frequency	353 MHz
Number of cells	47
Tank diameter	51.280 cm
Drift–tube diameter	10.850 cm
Bore diameter	1.0 cm
Average cell length	5.527 cm
Average drift–tube length	4.421 cm
Average gap length	1.105 cm
Overall tank length	259.76 cm
Face angle	1.4–6.0°
Stem diameter	1.905 cm
Post–coupler diameter	1.270 cm

The parameters of the structure are summarized in Table 4 and the variation of the permeability μ of the equivalent waveguide is shown in Table 5. Using curve fitting, the variation of μ along the axis was approximated by

$$\mu(z)/\mu_0 = 0.997248 + 1.66294 \times 10^{-5} z - 2.5149 \times 10^{-8} z^2 \tag{21}$$

Numerically integrating the transmission line equations, properly taking into account the absence of virtual stems in the end cells, we obtain a natural ramp of 21% as compared to the experimental value of 24%. With end faces displaced to change the resonant frequency by 225 kHz and then bring it back to the original value, as in Billen's experiments, Siddiqi *et al.* obtained the ramp shown in Figure 10. The results obtained by using the present transmission line model are shown to compare also very well with the experiment.

TABLE 5: The variation of the permeability m of the equivalent waveguide for CWDD DTL

cell no.	1	10	20	30	40
position(cm)	1.97	39.80	86.46	142.27	205.64
Δf (MHz)	1.3230	1.2158	1.1042	1.0010	0.9088
μ(z) (μ_0)	0.9973	0.9979	0.9985	0.9991	0.9996

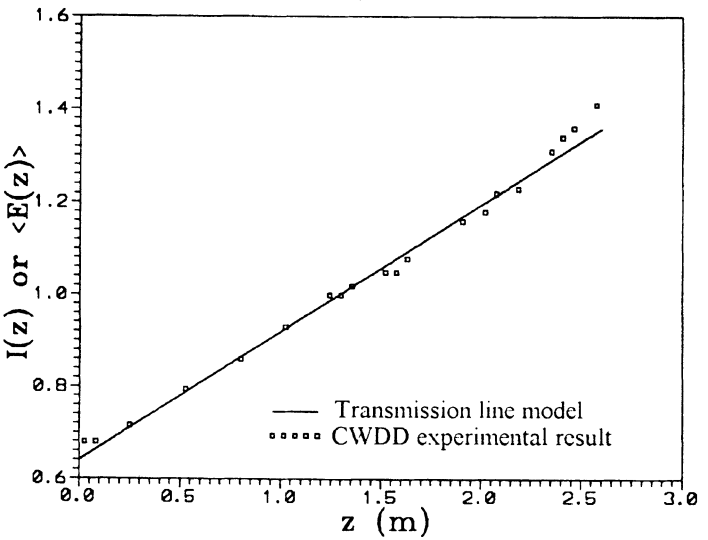

FIGURE 10: Comparison of the calculation results with CWDD DTL experimental data.

8 POST COUPLERS

The effect of post couplers in the context of transmission line representation can be obtained by modeling them as lumped element circuits.[13]

A. Post couplers in a constant gradient DTL

If the DTL structure is uniform and the accelerating field average over each cell is also independent of location (this corresponds to zero voltage, constant current on the equivalent transmission line), stabilization can be achieved by using straight posts. As was indicated above, since the post diameter is much smaller than one wavelength, the post can be represented by a reactive shunt network. Over a narrow frequency range in the neighborhood of the operating frequency, this network is a series L-C circuit as shown in Figure 11, The resonant frequency of this circuit is determined primarily by the length of the post, while the L/C ratio is set by the post diameter. The post impedance is given by

$$Z_p = j\omega L + \frac{1}{j\omega C} = j(L/C)^{1/2}\left(\frac{\omega}{\omega_p} - \frac{\omega_p}{\omega}\right) \tag{22}$$

where $\omega_p = 1/(LC)^{1/2}$ is the post resonant frequency. For an unperturbed tank, E_r or the transmission line voltage is zero and the shunt elements draw no net current. If the tank is perturbed, say, by moving the end faces, the voltage is no longer zero and a ramp would

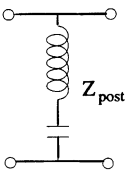

FIGURE 11: The equivalent circuit of a straight post in the DTL

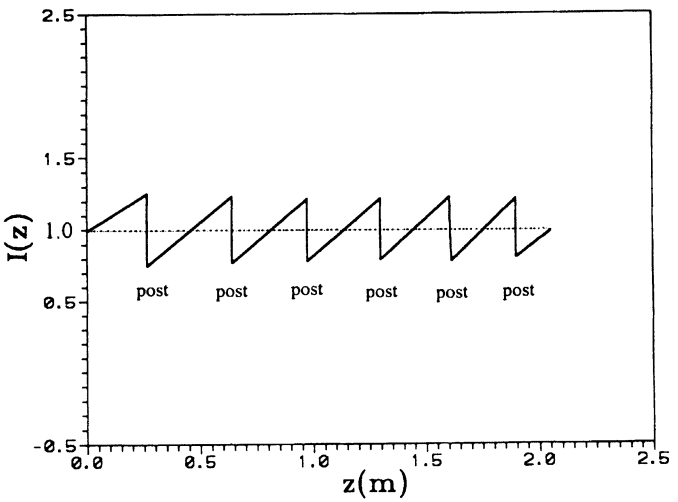

FIGURE 12: Posts in a DTL stabilized the fields against the perturbations.

result. The shunt elements then would draw current and the current (i.e. H_ϕ) distribution would have saw-tooth shape as shown in Figure 12. In order to stabilize the structure, i.e. to insure that the average current (and therefore average accelerating field) remain unchanged by the perturbation, the posts must be inductive at the operating frequency. Therefore the post resonant frequency must be below the actual operating frequency. This was previously shown by Shmoys *et al.*[14] and is in agreement with experiments by J. Ungrin[15] and by J.H. Billen.[16] Typical dependence of the gap voltage ratio on the post resonant frequency is shown in Figure 13. The effect of posts on the resonant frequencies of higher order modes is shown in Figure 14 and Table 6.

B. Posts in a ramp gradient linac

Clearly, a ramp can be established by deliberately detuning the end cells, To stabilize this ramp is more difficult than to stabilize a uniform field structure. It can be shown that the straight posts cannot accomplish this. Stabilization can be achieved by the use of posts

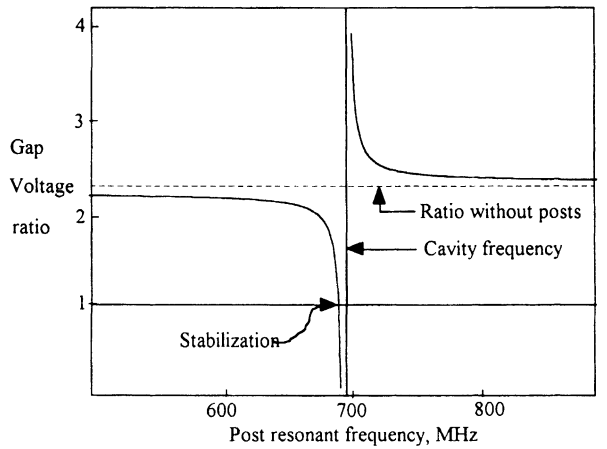

FIGURE 13: Ratio of maximum to minimum gap voltage for linac vs. post coupler resonant frequency

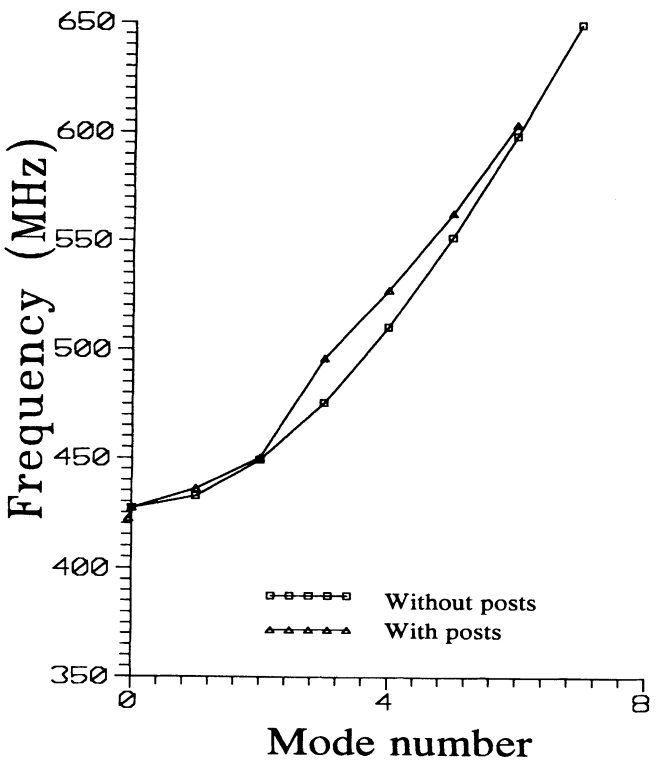

FIGURE 14: Resonant frequencies of higher order modes of linac of Table 1

TABLE 6: Resonant frequencies of higher order modes of linac of Table 1

Mode	Frequency (MHz) (without posts)	Frequency (MHz) (with 8 posts)
Post mode		422.193
Cut off	427.000	427.000
1	432.689	436.223
2	449.325	450.450
3	475.761	496.256
4	510.476	527.435
5	551.910	562.960
6	598.670	603.769
7	649.607	

with tabs or bent posts (see, e.g., Billen[17]). The bent post cannot be represented by the simple shunt network of Figure 11. It was found that the 2-port shown in Figure 15 can well represent it. This 2-port is inserted at the location of the post between sections of transmission line representing the linac structure between posts.

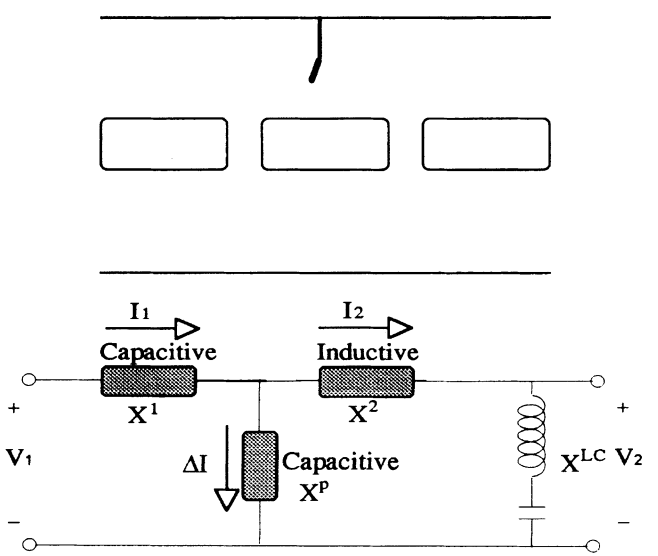

FIGURE 15: The bent post in the DTL and its equivalent circuits

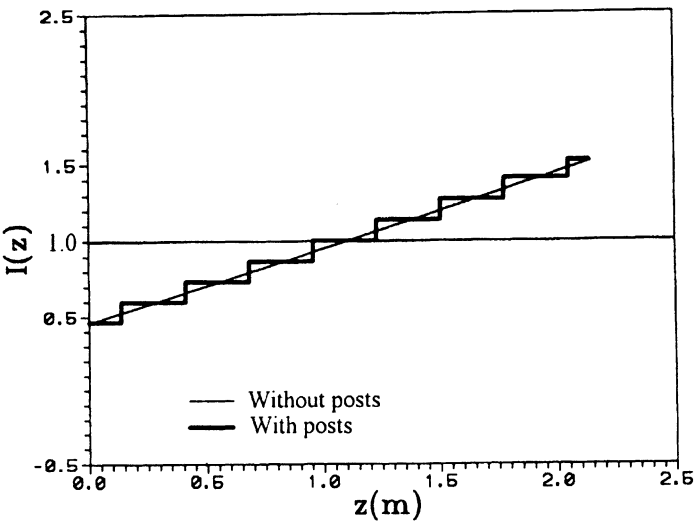

FIGURE 16: The current distributions in a DTL with and without posts

Using the parameters of the linac previously referred to, shown in Table 1, a stabilizing two-ports of the configuration of Figure 15 were synthesized. Different two-ports were required for each of the 8 posts used. The reactances of the nth post are each approximated by a linear function of frequency (over a narrow range) as:

$$X_n^K = X_{n0}^K + a_n^K (f - f_0) \tag{23}$$

where f_0 is the normal operating frequency and $k = 1, 2, p, LC$ (see Figure 15 and Table 8). We note that for $a_n > 0$, X_n obeys the Foster reactance theorem. The values obtained for the various locations are shown in Table 7. The resulting linac resonant frequencies are shown in Table 6; we see that the effect of post couplers is to increase the spacing between resonances. The current distribution in the transmission line model of this linac is shown in Figure 16. The effect of detuning by moving end faces of the linac is shown in Figure 17. Corresponding experimental results of Billen[13] are shown in Figure 18. We see that the transmission line circuit model shows good agreement with experiment.

9 CONCLUSION

We showed in this paper that a linac structure, including the effects of copper losses, beam loading, stems and feeds, can be well represented by transmission lines. The results obtained using the transmission line model compare very well with experimental results. One advantage of the transmission line model is that one can predict the effect of changes in the structure without resorting to calculating the field distribution in the entire linac using

TABLE 7: Equivalent circuit parameters for a post

n	Cell	a_n^1	a_n^2	a_n^p	a_n^{LC}	X_{n0}^1	X_{n0}^2	X_{n0}^p	X_n^{LC}
1	3	.19E–06	.17E–06	.23E–05	.54E–04	–79.630	73.757	–1000.00	107.98
2	9	.25E–06	.22E–06	.23E–05	.54E–04	–105.652	95.557	–1000.00	107.98
3	15	.28E–06	.25E–06	.23E–05	.54E–04	–118.133	105.652	–1000.00	107.98
4	21	.31E–06	.28E–06	.23E–05	.54E–04	–133.958	118.133	–1000.00	107.98
5	27	.36E–06	.31E–06	.23E–05	.54E–04	–154.679	133.958	–1000.00	107.98
6	33	.43E–06	.36E–06	.23E–05	.54E–04	–182.982	154.679	–1000.00	107.98
7	39	.52E–06	.43E–06	.23E–05	.54E–04	–223.964	182.982	–1000.00	107.98
8	45	.68E–06	.52E–06	.23E–05	.54E–04	–288.600	223.964	–1000.00	107.98

X_n^1		X_n^1		X_n^p		X_n^{LC}	
–150kHz	+150kHz	–150kHz	+150kHz	–150kHz	+150kHz	–150kHz	+150kHz
–79.677	–79.584	73.714	73.800	–1000.586	–999.415	94.513	121.443
–105.714	–105.590	95.501	95.612	–1000.586	–999.415	94.513	121.443
–118.203	–118.064	105.591	105.714	–1000.586	–999.415	94.513	121.443
–134.037	–133.880	118.064	118.203	–1000.586	–999.415	94.513	121.443
–154.769	–154.588	133.880	134.037	–1000.586	–999.415	94.513	121.443
–183.090	–182.875	154.588	154.770	–1000.586	–999.415	94.513	121.443
–224.095	–223.833	182.875	183.090	–1000.586	–999.415	94.513	121.443
–288.769	–288.431	223.833	224.095	–1000.586	–999.415	94.513	121.443

numerical codes, which is often impossible, or at least impractical. Response due to beam loading such as cavity detuning and field phase distribution etc. can also be calculated using the model. These are important for accelerators of high beam loading factors. The analysis on post couplers is shown to agree well with experiments. It provides the reason that an asymmetric structure is needed for a ramped gradient DTL.

ACKNOWLEDGEMENTS

This Research was performed under contract No. DNA 001-85-C-0182. We appreciate enlightening discussions with J.H. Billen, R.K. Cooper, S.P. Jachim, M. Lorello, S. Siddiqi, and T.P. Wrangler.

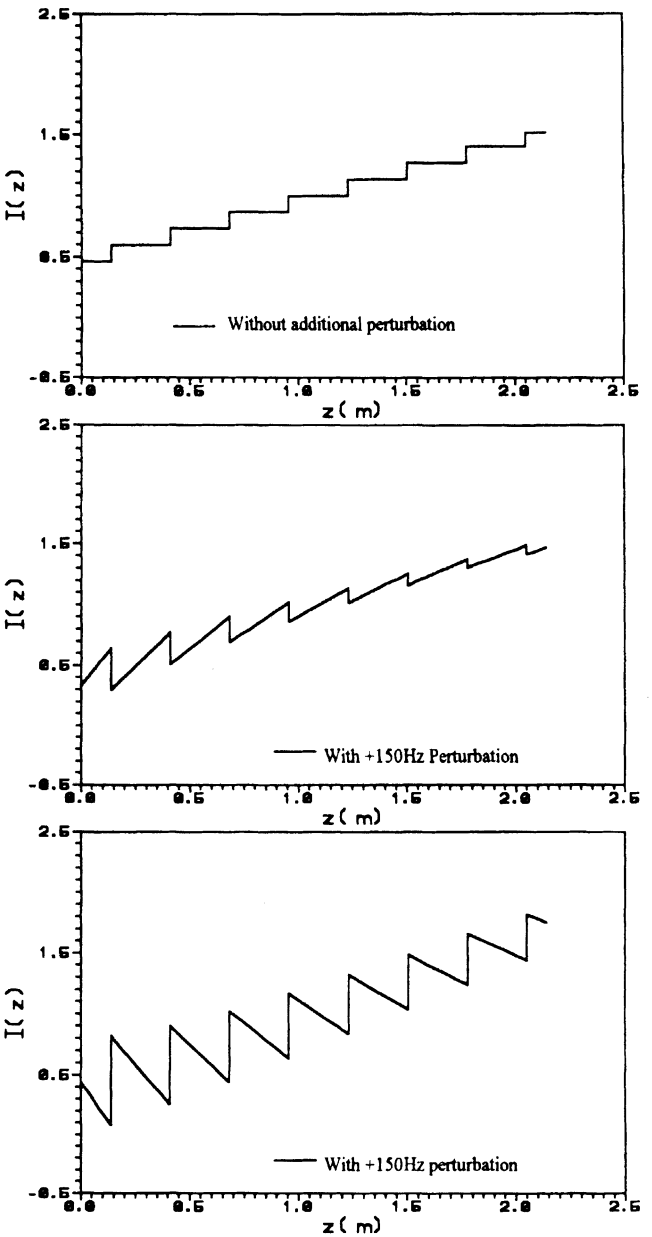

FIGURE 17: Stabilized fields for different perturbations in a DTL using transmission line model.

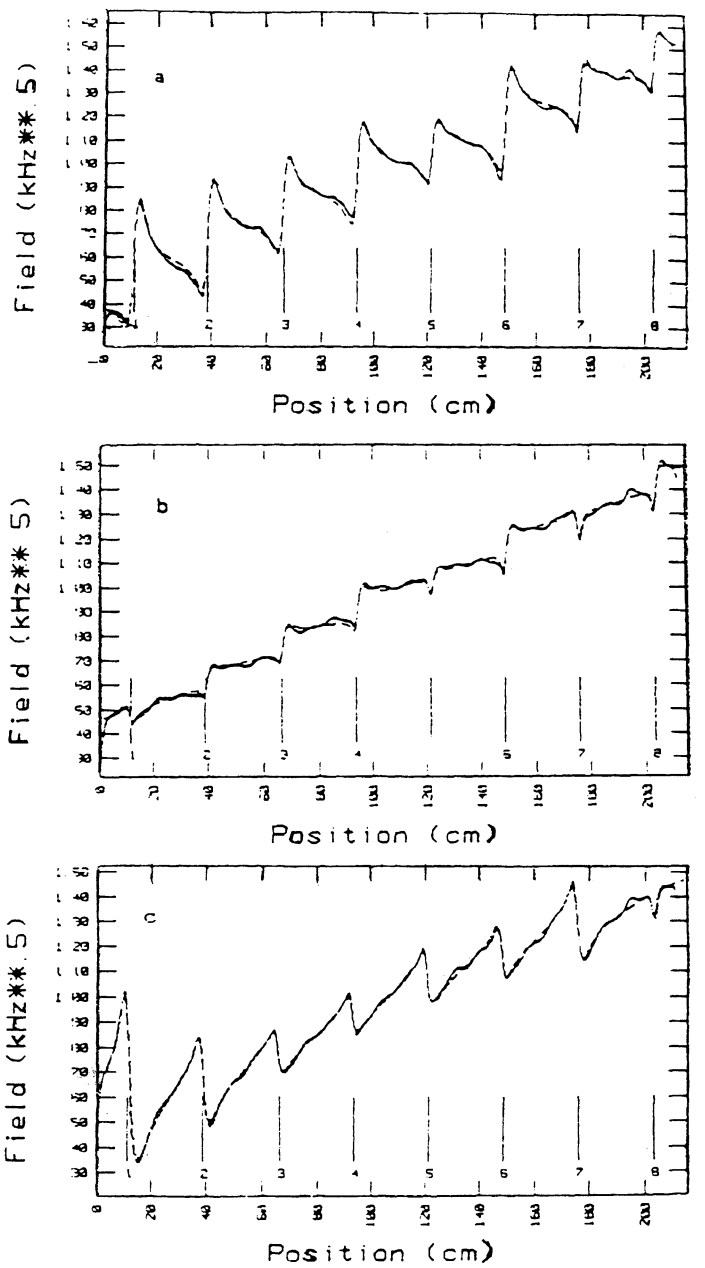

FIGURE 18: Field stabilization using posts by experimental arrangements carried out by J.H. Billen.

REFERENCES

1. K. Halbach and R.F. Hosinger, 'SUPERFISH – A Computer program for evaluation of RF cavities with cylindrical symmetry', *Particle Accelerators*, **7** (1976), 213–222.
2. J. Shmoys, R.M. Jones, and B.R. Cheo, 'Cascaded transmission line model for global DTL analysis', in *proc. 1988 Linear Accelerator Conf.*, pp. 332–334.
3. B.R. Cheo, J. Shmoys, M.-K. Ke, and R.M. Jones, 'Transmission line modeling of beam loading and other perturbations in an RFQ', *Particle Accelerators*, **39** (1992), 47–63.
4. A. Carne, "Low and Medium Energies Alvarez Structures", pp. 593–597, in *Proton Linear Accelerators*, edited by P.M. Lapostolle and A.L. Septier, North-Holland, Amsterdam, 1970.
5. M.-K. Ke, "Continuous Transmission Line Modeling for Low and Medium Energy Linacs: DTLs & RFQs", PhD Thesis, Jan, 1993, Polytechnic University, Brooklyn, New York.
6. L. Felsen and N. Marcuvitz, Radiation and Scattering of Waves (Prentice-Hall, Inc., Englewood Cliffs, New Jersey, 1973), pp. 86, 87, 183ff.
7. C.S. Taylor, "Radiofrequency Problem", pp. 912, in *Proton Linear Accelerators*.
8. C.S. Taylor, "Radiofrequency Problem", pp. 910, in *Proton Linear Accelerators*.
9. R.F. Harrington, *Time Harmonic Electromagnetic Fields* (McGraw-Hill, New York, 1961) pp. 106–116, 434–440.
10. J.H. Billen and D.E. McMurry, 'Low Power RF Modeling of the Drift Tube Linac for the Continuous Wave Deuteron Demonstrator', LANL Technical Memo, AT-1:89–789.
11. S. Siddiqi, I. Clarkson, M. Lorello, J. O'Toole, P. Fraser, S. Barbour, A. Todd, C. Paulson, S. Mendelsohn, J. Sredniawski, W. Shephard, and M. Cole, "Variable Ramped Gradient Drift Tube Linac Cold Model Tests", submitted to 16th International Linac Conference, Ottawa Ontario, Aug. 23–28, 1992.
12. M.K Ke, *op. cit.* pp. 19–20, Jan, 1993.
13. G. Dome, "Review and Survey of Accelerating Structures", pp. 701–709, in Proton Linear Accelerators.
14. J. Shmoys, R.M. Jones, and B.R. Cheo, "Cascaded Transmission Line Model for Global DTL Analysis", 1988 Linear Accelerator Conference, GEBAF, WE3-12.
15. J. Ungrin, S.O. Schriber, and R.A. Vokes, "Post-Coupler and Stem Current Measurements for High Current CW Drift-Tube Linacs", *IEEE Trans. On Nuclear Science*, Vol. NS-30, No.4, August 1983.
16. J.H. Billen, private communication.
17. J.H. Billen and A.H. Shapiro, "Post-Couplers Stabilization and Tuning of a Ramp-Gradient Drift-Tube Linac", *1988 Linear Accelerator Conference*, GEBAF, M03-36.